3.3.2. Calcium Silicate Samples

ICET Test #4 was the second test that included cal-sil insulation samples in addition to fiberglass samples. XRD/XRF results show the crystal structure and the chemical composition of the unused raw and unused baked cal-sil samples. Based on XRD results, both unused raw and unused baked cal-sil samples contained crystalline substances of tobermorite ($Ca_{2.25}(Si_3O_{7.5}(OH)_{1.5})(H_2O)$) and calcite ($CaCO_3$). XRF results indicated that the dominant elemental compositions of cal-sil include Si and Ca and small amounts of Al, Fe, Na, and Mg. There was no significant difference in elemental composition between raw and baked unused cal-sil. After being baked in a laboratory oven at 260°C for 72 hours, the raw cal-sil color changed from yellow to pink. The possible property changes of cal-sil after being baked include loss of water and oxidation of reductive species such as organic carbon, Fe(0), and Fe(II), as well as possible mineral and crystal structural changes. Specifically, oxidation of Fe(0) and Fe(II) into Fe_2O_3 is likely responsible for the baked cal-sil's turning pink.

Both raw and baked cal-sil samples were submerged in the tank throughout the test. No significant differences were found between the raw and baked cal-sil, or between the exterior and the interior. EDS results show that both raw and baked cal-sil were composed primarily of O, Si, Ca, Na, Al, C, Mg, and Fe. Due to the granular shape of cal-sil particles, it is difficult to distinguish whether the particles are foreign deposits or they are the cal-sil particles themselves. Figures 3-86 through 3-97 show cal-sil results.

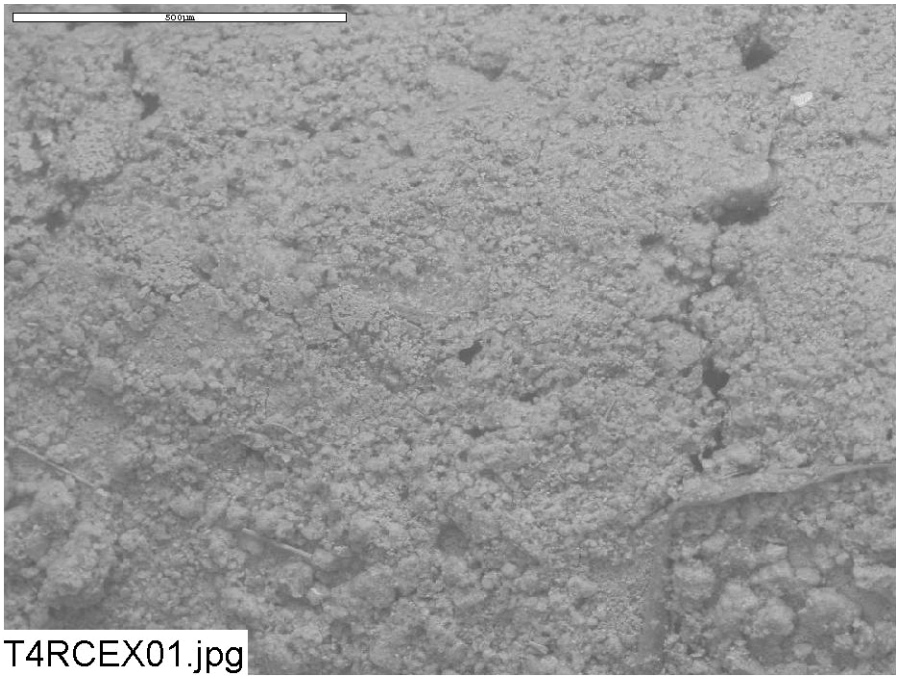

Figure 3-86. ESEM image magnified 100 times for a Test #4, Day-30 low-flow exterior raw cal-sil sample. (T4RCEX01.jpg)

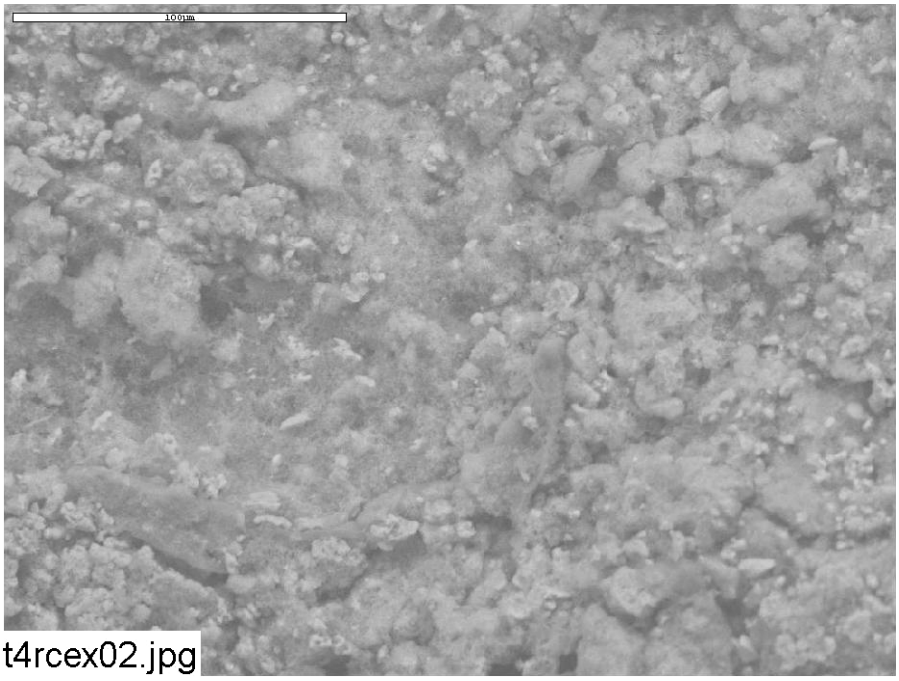

Figure 3-87. ESEM image magnified 500 times for a Test #4, Day-30 low-flow exterior raw cal-sil sample. (t4rcex02.jpg)

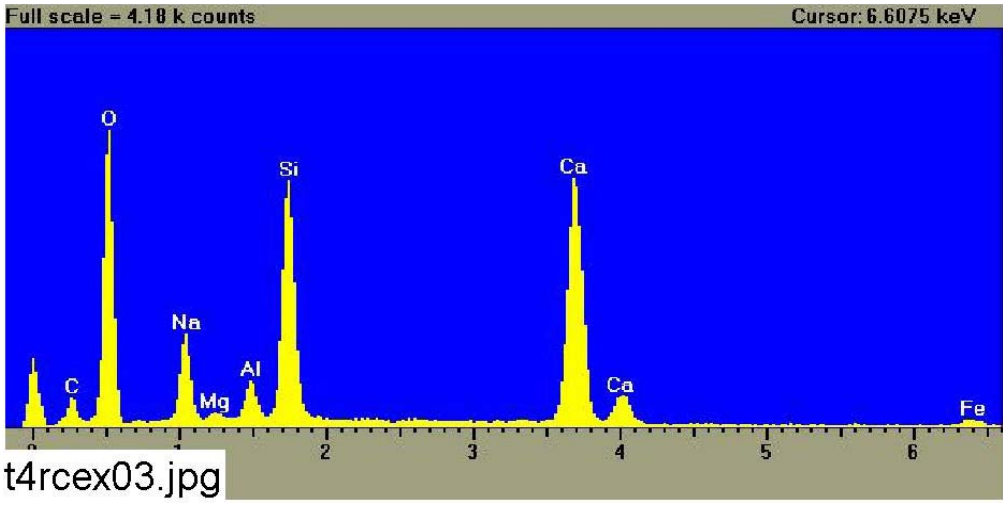

Figure 3-88. EDS counting spectrum for the whole image shown in Figure 3-87. (t4rcex03.jpg)

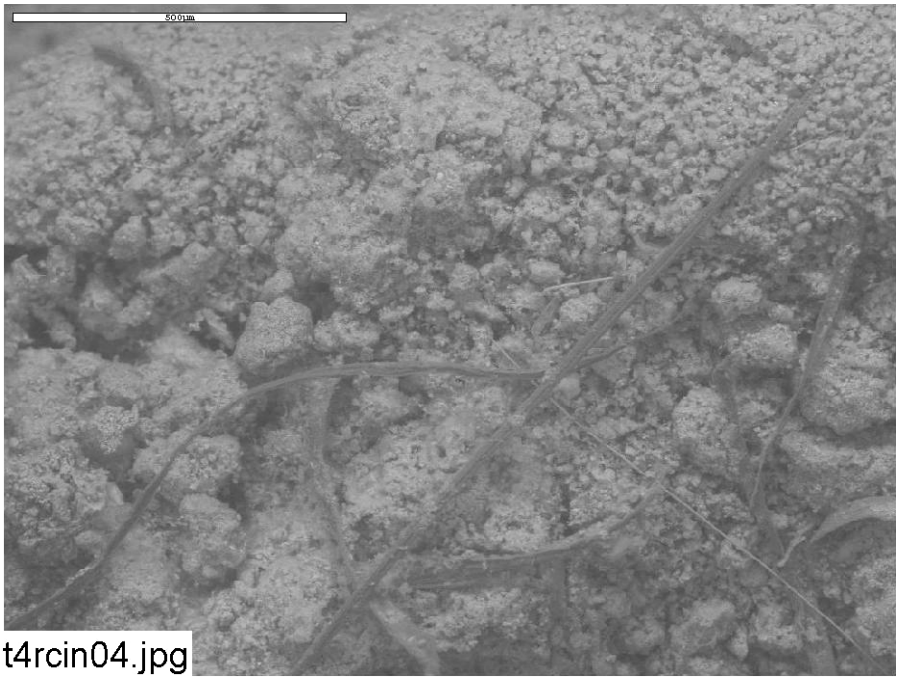

Figure 3-89. ESEM image magnified 100 times for a Test #4, Day-30 low-flow interior raw cal-sil sample. (t4rcin04.jpg)

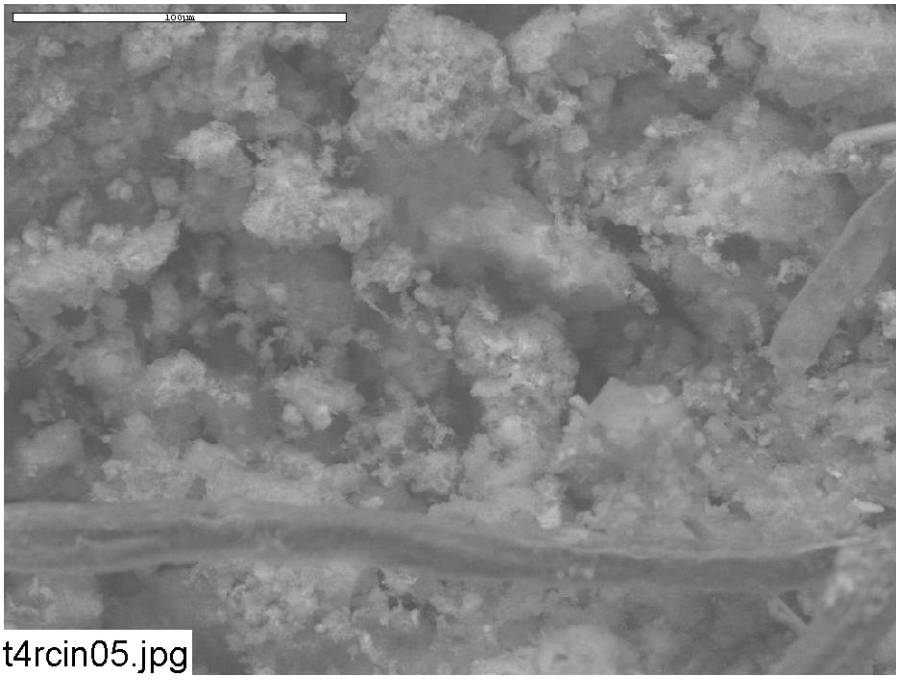

Figure 3-90. ESEM image magnified 500 times for a Test #4, Day-30 low-flow interior raw cal-sil sample. (t4rcin05.jpg)

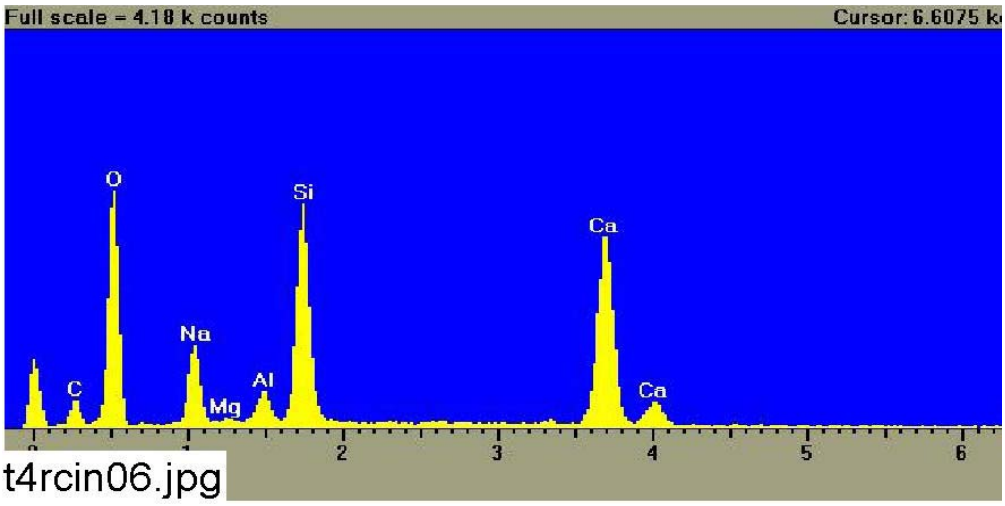

Figure 3-91. EDS counting spectrum for the whole image shown in Figure 3-90. (t4rcin06.jpg)

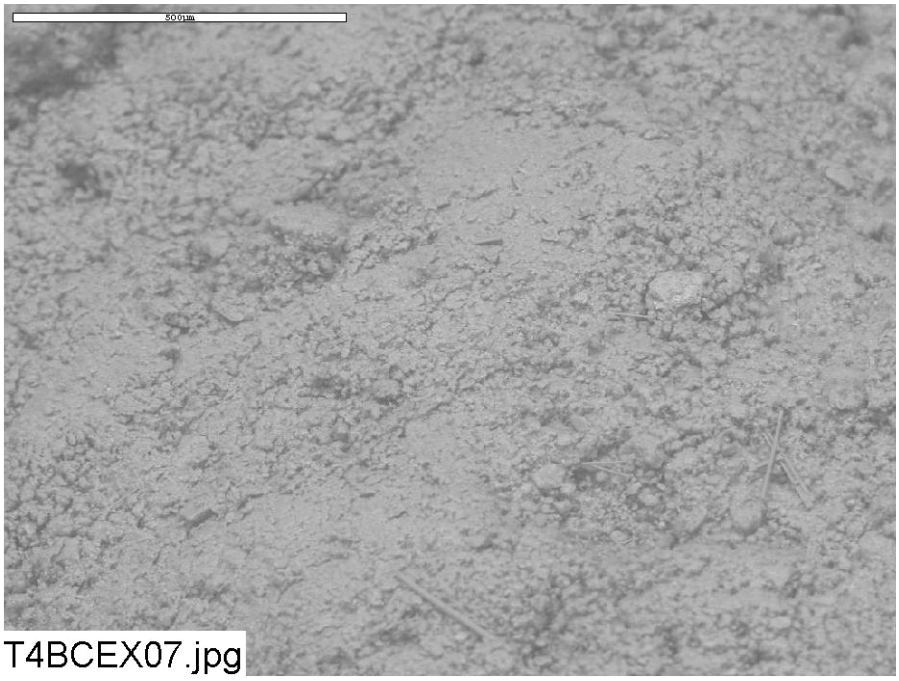

Figure 3-92. ESEM image magnified 100 times for a Test #4, Day-30 low-flow exterior baked cal-sil sample. (T4BCEX07.jpg)

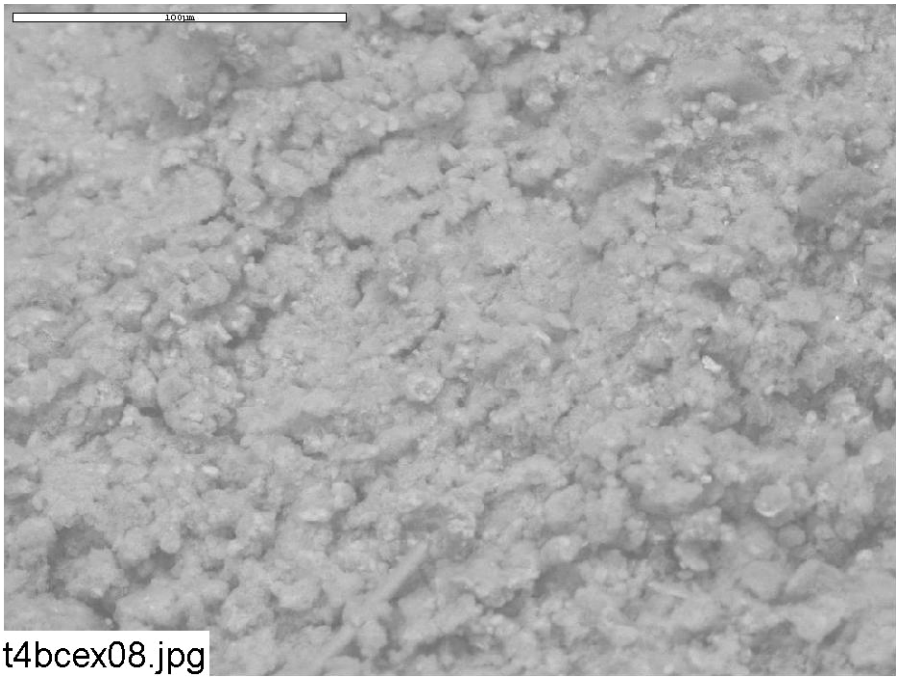

Figure 3-93. ESEM image magnified 500 times for a Test #4, Day-30 low-flow exterior baked cal-sil sample. (t4bcex08.jpg)

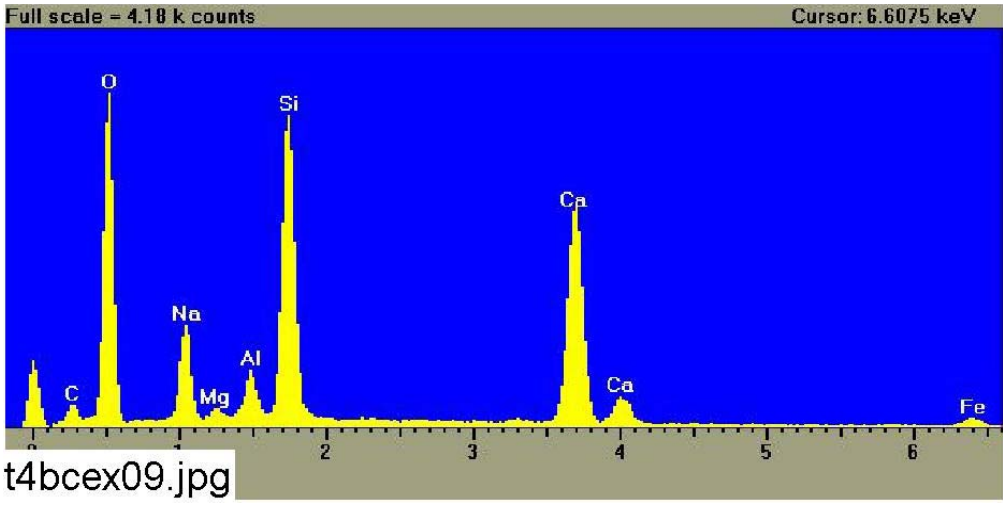

Figure 3-94. EDS counting spectrum for the whole image shown in Figure 3-93. (t4bcex09.jpg)

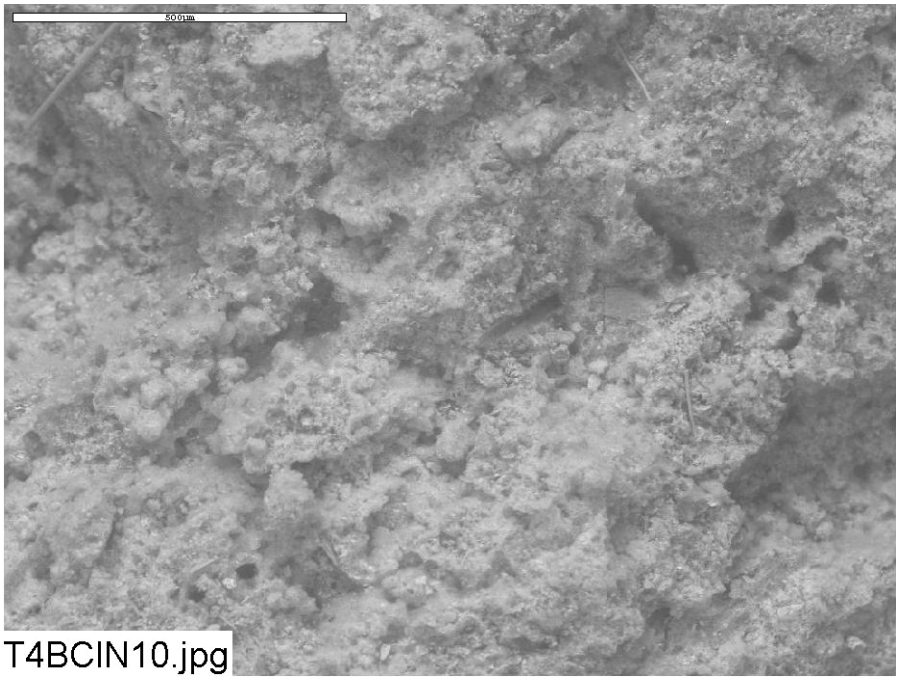

Figure 3-95. ESEM image magnified 100 times for a Test #4, Day-30 low-flow interior baked cal-sil sample. (T4BCIN10.jpg)

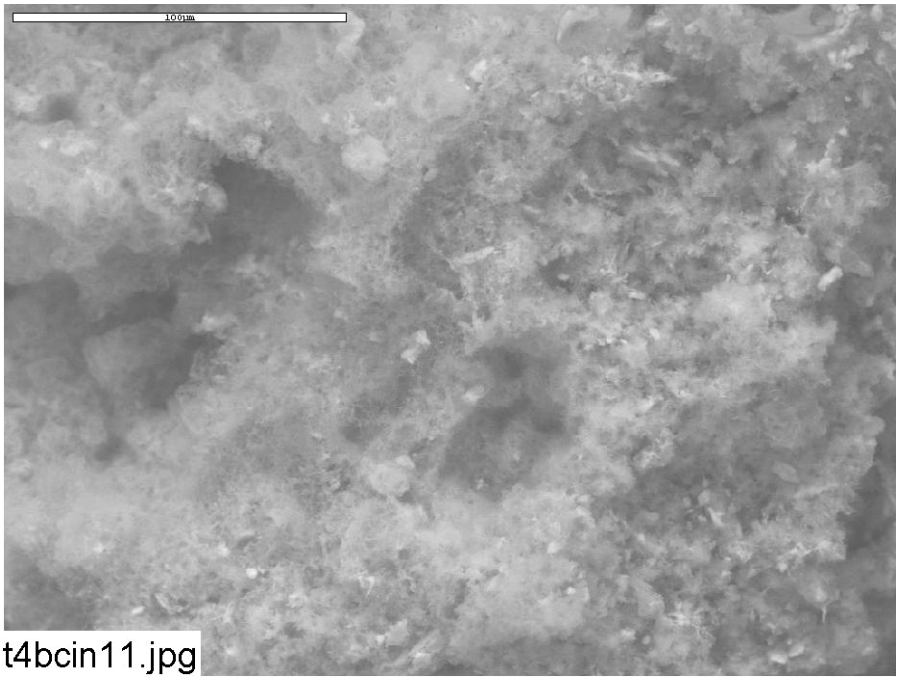

Figure 3-96. ESEM image magnified 500 times for a Test #4, Day-30 low-flow interior baked cal-sil sample. (t4bcin11.jpg)

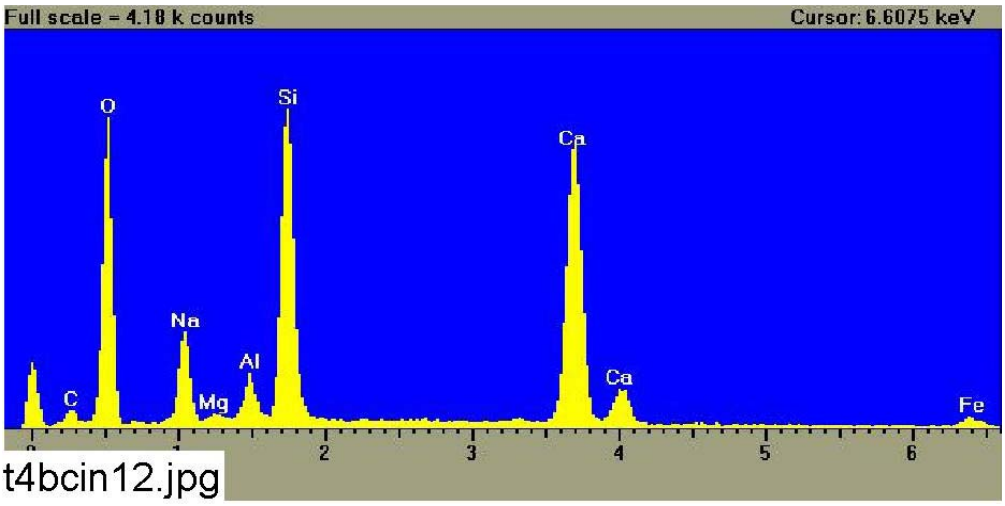

Figure 3-97. EDS counting spectrum for the whole image shown in Figure 3-95. (t4bcin12.jpg)

3.4. Metallic and Concrete Coupons

3.4.1. Weights and Visual Descriptions

3.4.1.1. Submerged Coupons

Examination of the 40 submerged coupons provides insights into the nature of the chemical kinetics that occurred during this 30-day test. The physical change that these coupons experienced is determined through both visual evidence and weight measurement of each coupon before and after the test. Pre-test pictures were taken of the coupons when they were received and before insertion in the racks. Post-test pictures were taken several days after the racks had been removed from the tank. All racks with coupons still inserted were staged to allow complete drying of the coupons before the post-test pictures. The coupons were placed in a low-humidity room and allowed to air dry. All coupons were also weighed before they were inserted into the tank and after the 30-day test was completed.

There are three submerged aluminum coupons in each test. Figures 3-98 through 3-100 display the pre- and post-test pictures of those coupons that were in Test #4. The relative locations of the aluminum coupons from east to west of the tank are: Al-239, Al-238, and Al-237. Al-239 and Al-238 were the two aluminum coupons that were isolated next to the concrete coupon. There were no visual differences between the three coupons after they were removed from the tank. The overall appearance of the aluminum coupons did not significantly change from their pre-test appearance. The post-test coupons appeared to have a light film on them and had lost their pre-test shiny appearance.

Figure 3-98. Al-237 submerged, pre-test (left) and post-test (right).

Figure 3-99. Al-238 submerged, pre-test (left) and post-test (right).

Figure 3-100. Al-239 submerged, pre-test (left) and post-test (right).

Figures 3-101 through 3-103 present the pre- and post-test pictures of three submerged galvanized steel coupons. The galvanized steel coupons did not experience any significant observable change. The coupons appeared to be relatively clean and the only noticeable marks of any sort are the circular marks caused by the racks that they are mounted in. GS-130 does appear to have some particle deposition that is concentrated mainly on the bottom corners and on the top where the coupon resides in the rack.

Figure 3-101. GS-130 submerged, pre-test (left) and post-test (right).

Figure 3-102. GS-132 submerged, pre-test (left) and post-test (right).

Figure 3-103. GS-134 submerged, pre-test (left) and post-test (right).

Figures 3-104 and 3-105 present the pre- and post-test pictures of two submerged inorganic zinc (IOZ) coated steel coupons. Both submerged IOZ coated steel coupons have similar, light particle depositions. There is a small accumulation of a white precipitate that originates mostly from the points of contact with the racks. However on IOZ-233, the particles seem to be distributed over the majority of the surface of the

coupon. This coupon was the westernmost IOZ coupon in the rack in relation to the others.

Figure 3-104. IOZ-233 submerged, pre-test (left) and post-test (right).

Figure 3-105. IOZ-234 submerged, pre-test (left) and post-test (right).

Figures 3-106 and 3-107 present the pre- and post-test pictures of two submerged copper coupons. The copper coupons were mainly unchanged. Like the other coupons, there is a very light concentration of particulate deposits in the areas where the coupons contact the rack.

Figure 3-106. Cu-548 submerged, pre-test (left) and post-test (right).

Figure 3-107. Cu-572 submerged, pre-test (left) and post-test (right).

Figure 3-108 presents the pre- and post-test pictures of the submerged carbon steel coupon. Other than some discoloration, there was no change. There was a small amount of rust on the bottom corners.

Figure 3-108. US-17 submerged, pre-test (left) and post-test (right).

Figure 3-109 presents the pre- and post-test pictures of the submerged concrete coupon. The post-test concrete coupon exhibits a brownish color.

Figure 3-109. Conc-004 submerged, pre-test (left) and post-test (right).

Table 3-2 presents the pre- and post-test weight data for each representative submerged coupon.

Table 3-2. Weight Data for Submerged Coupons

Type	Coupon No.	Pre-Test Wt. (g)	Post-Test Wt. (g)	Net Gain/Loss
Al	237	392.1	391.9	-0.2
Al	238	393.1	393.3	0.2
Al	239	392.8	392.8	0.0
GS	130	1042.9	1042.9	0.0
GS	132	1062.1	1062.3	0.2
GS	134	1028.5	1029.0	0.5
IOZ	233	1610.9	1612.6	1.7
IOZ	234	1635.7	1637.9	2.2
CU	548	1300.7	1300.9	0.2
CU	572	1316.7	1316.9	0.2
US	17	1017.4	1017.6	0.2
Conc	04	7950.7	8190.3	239.6

The aluminum coupons average weight differential was zero. This supports the observation that there was little particle deposition. The galvanized steel coupons gained an average of 0.23 g, and the coated steel coupons gained an average of 2.0 g. Both representative copper coupons gained 0.2 g, and the carbon steel coupon also gained 0.2 g. The concrete coupon gained 239.6 g, a gain of 3% of its original weight. The concrete coupon was weighed after sitting in an air environment for one week.

3.4.1.2. Unsubmerged Coupons

Figures 3-110 and 3-111 show the pre- and post-test pictures of two unsubmerged aluminum coupons. Each unsubmerged aluminum coupon accumulated a white particle deposition along with some areas of a brownish color. This coating caused the surface of the aluminum coupons to become coarse and rough. The photo of Al-229 shows that most of the surface is coated with the particle deposition, however, in the upper right hand corner the surface is relatively smooth with a color change observable. This is likely caused by uneven spray on the coupons. Even though the four spray nozzles were set to spray uniformly across their spray radius, the spray was not a perfect mist. There were some non-uniform areas, and the positions of the six coupon racks also interfered with the sprays. Al-003 was loaded in Rack 2 (bottom tier, southernmost), and Al-229 was loaded in Rack 7 (upper tier, northernmost).

Figure 3-110. Al-003 unsubmerged, pre-test (left) and post-test (right).

Figure 3-111. Al-229 unsubmerged, pre-test (left) and post-test (right).

Figures 3-112 and 3-113 show the pre- and post-test pictures of two unsubmerged galvanized steel coupons. There was some white deposition on the surface of these coupons although it was in small amounts. The post-test coupons were relatively clean,

with little change. GS-33 was mounted in Rack 3 (bottom tier, middle rack), and GS-91 was mounted in Rack 6 (upper tier, middle rack).

Figure 3-112. GS-33 unsubmerged, pre-test (left) and post-test (right).

Figure 3-113. GS-91 unsubmerged, pre-test (left) and post-test (right).

Figures 3-114 and 3-115 present the pre- and post-test pictures of two unsubmerged copper coupons. All of the copper coupons had vertical water marks that were caused by water flowing downward on the coupon surface during the spray portion of the test. The copper coupons did not appear to accumulate any particle deposition. Cu-536 was mounted in Rack 2 (bottom tier, southernmost), and Cu-584 was mounted in Rack 7 (upper tier, northernmost).

Figure 3-114. Cu-536 unsubmerged, pre-test (left) and post-test (right).

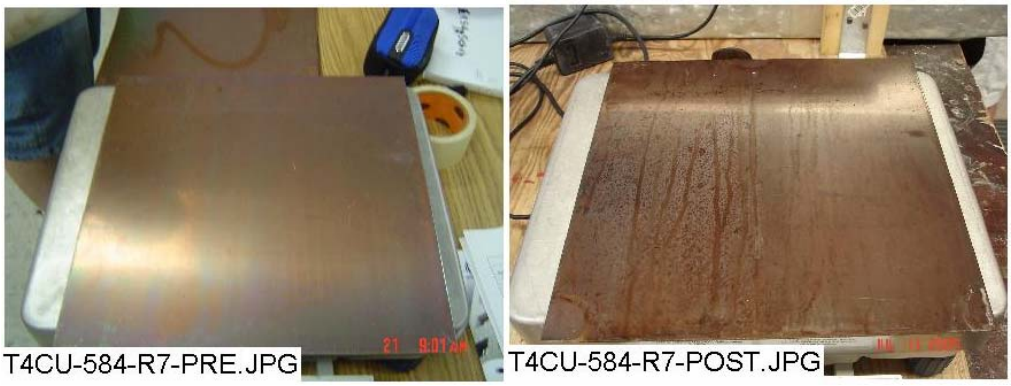

Figure 3-115. Cu-584 unsubmerged, pre-test (left) and post-test (right).

Figures 3-116 and 3-117 present the pre- and post-test pictures of two unsubmerged inorganic zinc coated steel coupons. IOZ-263 was mounted in Rack 4 (bottom tier, northernmost) and IOZ-275 was mounted in Rack 5 (upper tier, northernmost).

Figure 3-116. IOZ-263 unsubmerged, pre-test (left) and post-test (left).

Figure 3-117. IOZ-275 unsubmerged, pre-test (left) and post-test (right).

Figure 3-118 presents the pre- and post-test pictures of one unsubmerged carbon steel coupon. US-16 was mounted in Rack 6 (upper tier, middle rack).

Figure 3-118. US-16 unsubmerged, pre-test (left) and post-test (right).

Table 3-3 presents the pre- and post-test weight data for each representative unsubmerged coupon.

Table 3-3. Weight Data for Unsubmerged Coupons

Type	Coupon No.	Pre-Test Wt. (g)	Post-Test Wt. (g)	Net Gain/Loss
Al	003	391.2	391.7	0.5
Al	229	392.8	394.5	1.7
GS	33	1046.6	1046.6	0.0
GS	91	1030.8	1030.6	-0.2
IOZ	263	1662.0	1662.7	0.7
IOZ	275	1655.0	1657.0	2.0
CU	536	1319.2	1319.3	0.1
CU	584	1334.2	1333.7	-0.5
US	16	1024.1	1023.7	-0.4

The aluminum coupons gained an average of 1.1 g, and the galvanized steel coupons lost an average of 0.1 g. The coated steel coupons average weight gain was 1.4 g, and the copper coupons average weight difference was –0.2 g. The carbon steel coupon lost 0.4 g.

Table 3-4 displays the mean weight gain/loss summary in grams for all of the submerged coupons. Table 3-5 displays the mean weight gain/loss summary in grams for all of the unsubmerged coupons by rack.

Table 3-4. Mean Gain/Loss Data for All Submerged Coupons (g)

Coupon Type	Mean Gain - Loss (g)
AL	0.0
GS	0.3
CU	0.2
IOZ	2.3
US	0.2
Concrete	239.6

Table 3-5. Mean Gain/Loss Data for All Unsubmerged Coupons (g)

Mean Gain-Loss Per Coupon Type (g)					
Rack No.	**AL**	**GS**	**CU**	**IOZ**	**US**
2	-0.3	0.8	-0.4	0.8	n/a
3	0.2	1.1	0.2	0.3	n/a
4	-0.4	0.9	-0.2	0.7	-0.8
5	0.1	2.0	<0.1	1.9	n/a
6	-0.5	0.7	-0.4	0.9	-0.4
7	-0.3	0.9	-0.3	1.7	n/a
Overall	0.6	0.2	0.3	1.1	-0.4

3.4.2. SEM Analyses

3.4.2.1. Submerged Coupons

During the ICET tests, trace metal cations may be released from the submerged metal coupon surfaces due to corrosion effects. Subsequently, the released metal cations may complex with the anions from the solution through electrostatic interactions with anions such as OH^-, SiO_3^{2-}, and CO_3^{2-}. More complicated, the complexed anions may attract other cations from the solution, such as Ca^{2+}, Mg^{2+}, Al^{3+}, Cu^{2+}, Zn^{2+}, and H^+. As a result, corrosion products (deposits) are formed and may continuously grow on the metal coupon surfaces. The thickness of the deposits were observed to be in the range of millimeters. The adherence between the metal coupons and the deposits is through chemical bonds, which are much stronger than van der Waals forces. Due to the vertical

orientation of the metal coupons in the tank (with a small horizontal cross-sectional area), the deposits on the metal coupon surface are likely of chemical origin, rather than being the result of particles settling on the surface.

According to SEM/EDS results, the dominant corrosion products on the submerged Al coupons are likely aluminum hydroxide with other substances containing Si, Ca, O, and C. For submerged Cu coupons, the possible corrosion products include CuO, $Cu_2(CO_3)(OH)_2$, and substances containing Ca, Si, Al, and O. For the submerged galvanized steel coupons, the possible corrosion products are oxides, hydroxides, silicate, and carbonate compounds of Zn, Ca, and Al. For the submerged steel coupon, the possible corrosion products include oxide, hydroxide, silicate, and carbonate compounds of Fe and Ca and compounds composed of Fe, Si, Ca, O, and Al.

3.4.2.2. Unsubmerged Coupons

The unsubmerged coupons were affected by the testing solution only during the 4-hour spray phase on the first day of the test and, following that, were affected by water vapor throughout the test.

According to SEM/EDS results, the dominant corrosion products on the unsubmerged Al coupons are likely aluminum hydroxide and/or aluminum oxide, and other corrosion products containing Si, Ca, O, and C. For unsubmerged Cu, the corrosion products on the coupon surface are likely CuO. The corrosion products were composed of C, O, Ca, Si, and Cl on the unsubmerged galvanized steel coupon surface. For the unsubmerged steel coupon, the likely corrosion products are Fe_2O_3, $Fe(OH)_3$, and $Fe_2(CO_3)_3$.

Appendix F contains the SEM data for the coupons.

3.5. Sedimentation

Sediment was collected from the tank bottom after the test solution was drained. It consisted of a particulate sediment that covered the entire tank bottom. Figure 3-119 shows some of this sediment. In addition, Figure 3-120 shows the tank bottom with the sediment, after the samples were removed. Figure 3-121 shows the top of the drain screen with the drain collar surrounded by sediment, and Figure 3-122 shows the drain screen and drain collar after removal from the tank. Figure 3-123 shows the birdcage sitting on top of a basket of cal-sil after the tank was drained. The cal-sil baskets sat on top of the sediment, and thus, the birdcage was not in direct contact with the sediment.

The SEM/EDS and XRD/XRF analyses provided information on the morphology and composition of Test #4 sediment. EDS results show that more than 84% of the sediment was composed of Si, Ca, and O. Consistently, XRF result shows that Si, Ca, and O are the major elements in the composition of the sediment, plus small amounts of Na, Al, Fe, and Mg.

Based on XRD results, the sediment sample contained crystalline substances of tobermorite ($Ca_{2.25}(Si_3O_{7.5}(OH)_{1.5})(H_2O)$) and $Ca_4(Si_6O_{15}(OH)_2)(H_2O)_5$) as well as calcite ($CaCO_3$), which are the same as unused raw or unused baked cal-sil samples. Considering the collective evidence from the EDS, XRF, and XRD analyses, it is likely that the sediment was composed of a significant amount of cal-sil debris, including both raw and baked cal-sil. It should be noted that other deposits such as fiberglass debris and corrosion products may also contribute to the sediments and can not be ruled out.

Figures 3-124 through 3-129 and Table 3-6 provide ESEM/EDS and XRD/XRF analysis results. The complete Day-30 sediment analyses are given in Appendix G.

Figure 3-119. Sediment removed from the tank.

Figure 3-120. Sediment on the tank bottom.

Figure 3-121. Drain collar surrounded by sediment on the tank bottom.

Figure 3-122. Drain collar and drain screen removed from the tank.

Figure 3-123. Birdcage and cal-sil baskets after the tank was drained.

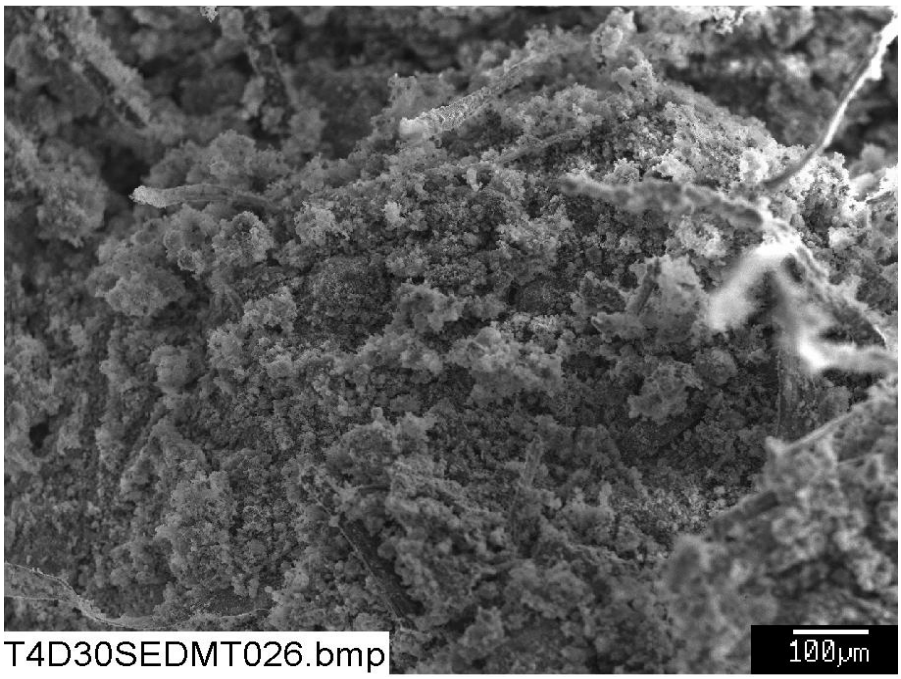

Figure 3-124. SEM image magnified 100 times for a Test #4, Day-30 sediment sample at the bottom of the tank. (T4D30SEDMT026.bmp)

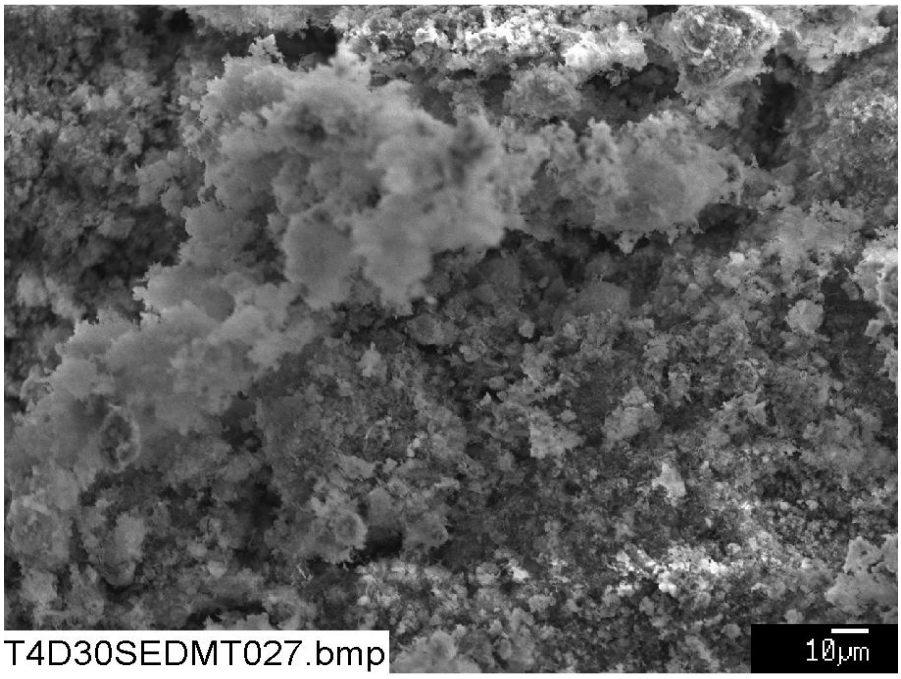

Figure 3-125. SEM image magnified 500 times for a Test #4, Day-30 sediment sample at the bottom of the tank. (T4D30SEDMT027.bmp)

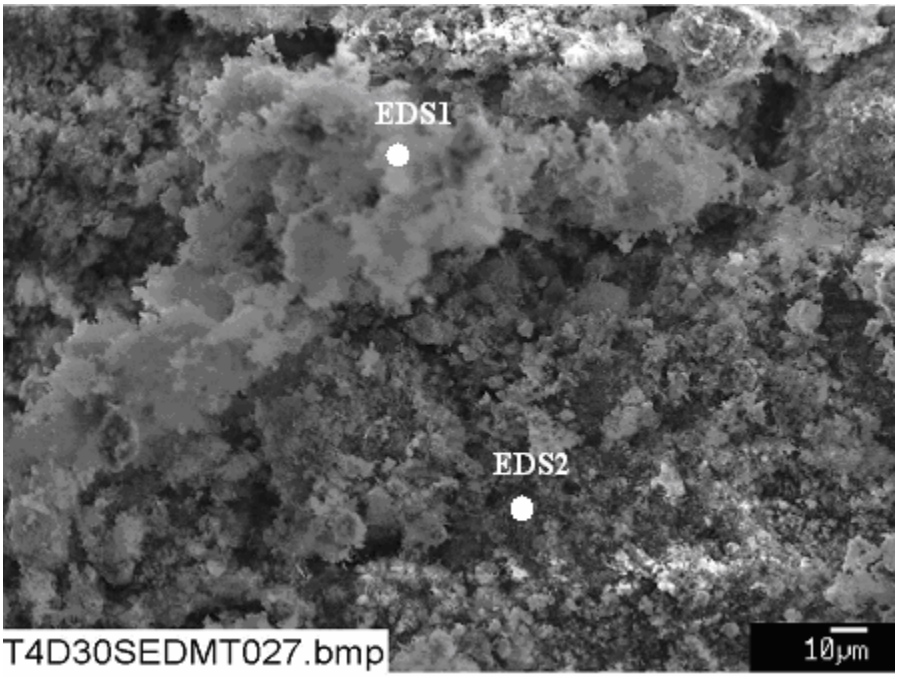

Figure 3-126. Annotated SEM image magnified 500 times for a Test #4, Day-30 sediment sample at the bottom of the tank. (T4D30SEDMT027.bmp)

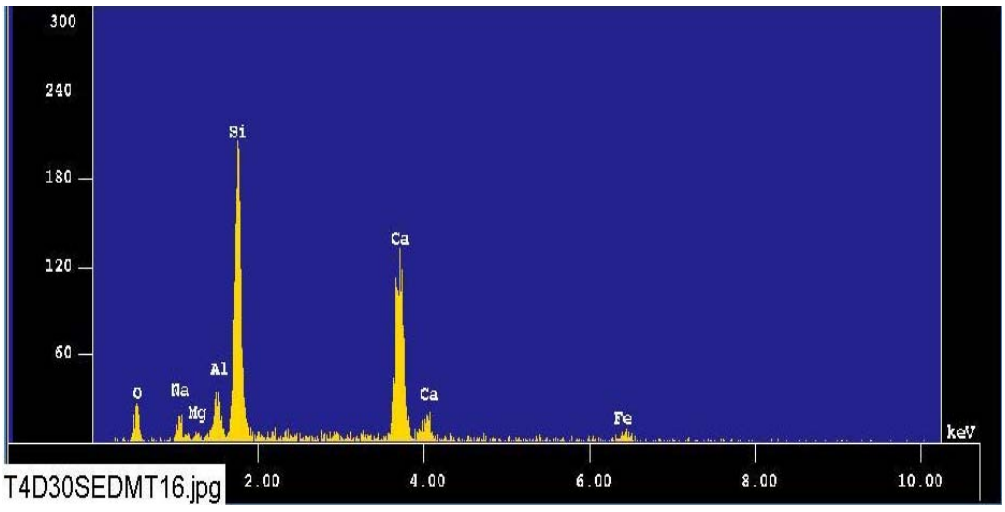

Figure 3-127. EDS counting spectrum for the white snow like deposits (EDS1) shown in Figure 3-126. (T4D30SEDMT16.jpg)

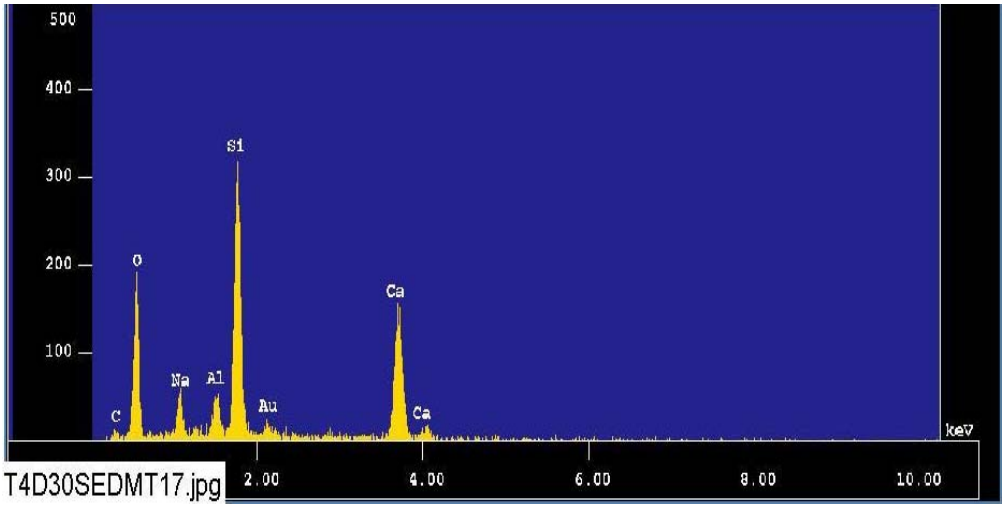

Figure 3-128. EDS counting spectrum for the dark deposits (EDS2) shown in Figure 3-126. (T4D30SEDMT17.jpg)

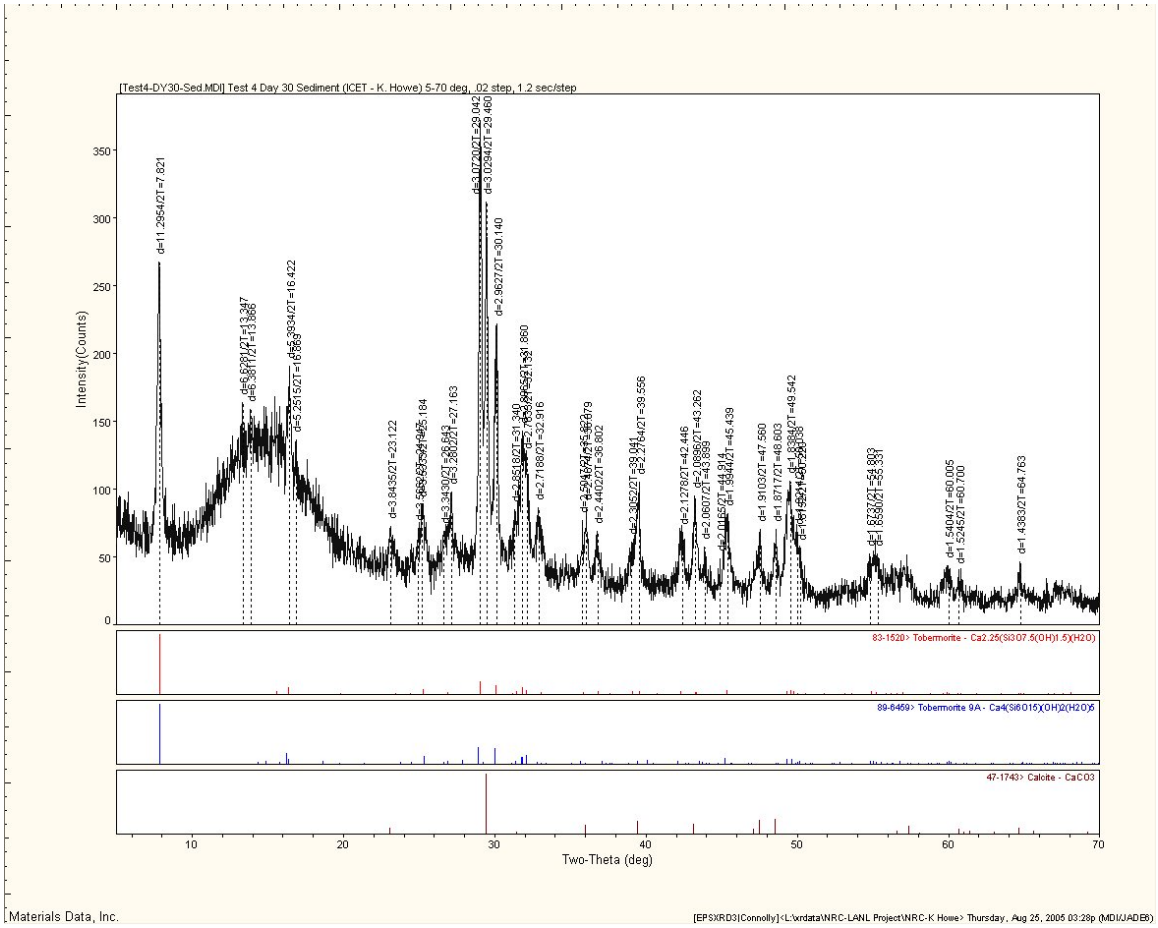

Figure 3-129. XRD result of the possible matching crystalline substances in Test #4, Day-30 sediment.

Table 3-6. Dry Mass Composition of Test #4, Day-30 Sediment by XRF Analysis

First row is chemical component; second row is mass composition (%).

SiO_2	TiO_2	Al_2O_3	Fe_2O_3	FeO	MnO	MgO	CaO	Na_2O	K_2O	$H_20(-)$	$H_2O(+)CO_2$	P_2O_5	Total
34.20	0.18	4.78	2.18	0.00	0.06	0.66	28.58	5.05	0.24	1.25	23.55	0.15	100.88

3.6. Precipitates

Test #4 was markedly different from Test #1 in that no precipitate was found in the test solution, even after it cooled to room temperature. Based on a series of bench-top controlled experiments, the white precipitate observed in Test #1 contained a significant amount of aluminum. The aluminum concentration of the Test #1 solution was as high as 350 mg/L. However, the aluminum in the Test #4 solution occurred only in trace amounts for 2 days and then was below its detection limit.

3.7. Deposition Products

The deposition of debris/corrosion products in the tank after it was drained was observed on the submerged objects in the tank. These corrosion/deposition products, which looked like a fine powder, were collected for analysis. Those collected were from the submerged CPVC coupon rack. SEM/ EDS results indicated that these fine powders were mainly composed of O, Ca, Si, Na, Al, and C. The high content of Ca and Si suggests that the powders were likely from cal-sil and fiberglass debris.

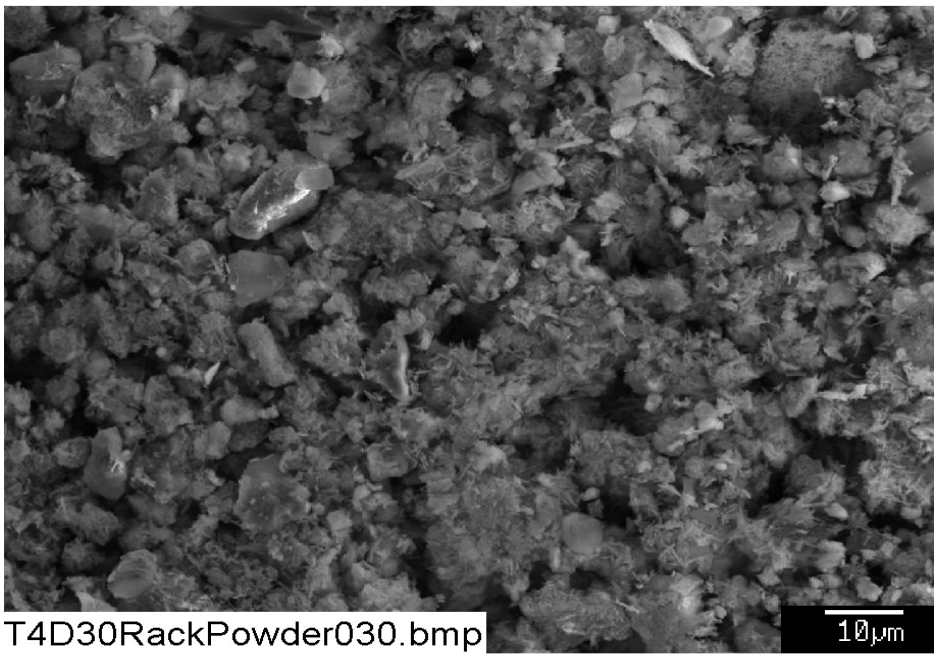

Figure 3-130. SEM image magnified 1000 times for a Test #4, Day-30 fine powder on the submerged rack. (T4D30RackPowder030.bmp)

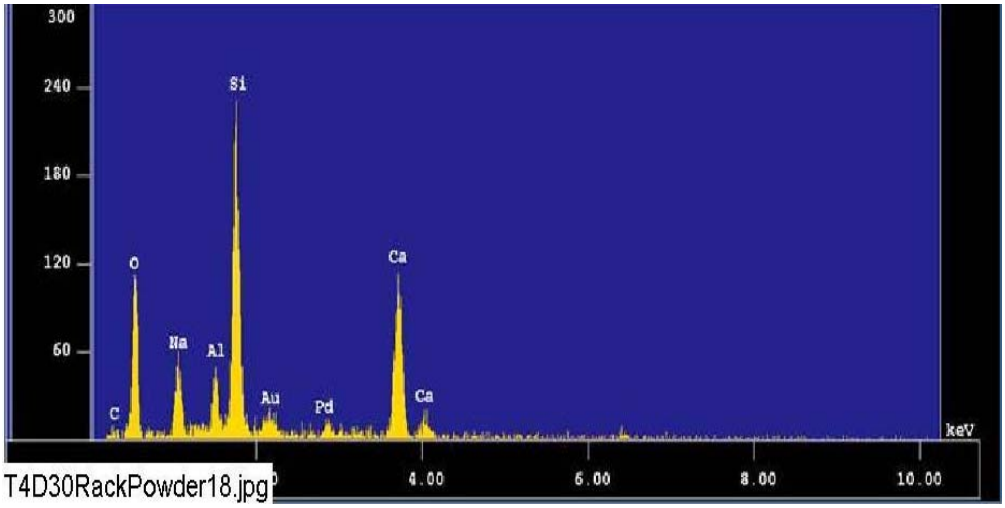

Figure 3-131. EDS counting spectrum for the particles (whole image) shown in Figure 3-130. (T4D30Rackpowder18.jpg)

3.8. Gel Analysis

In ICET Test #3, one significant phenomenon was the presence of white gel-like precipitates in the test solution, especially during and after the injection of TSP on the first day of the test. When Test #3 was shut down, deposits of the pinkish-white gel-like precipitates were observed on the top of the birdcage and on other objects on the tank's bottom. Test #4 had cal-sil and fiberglass samples as did Test #3, however, Test #4 used NaOH instead of TSP. No gel-like material was observed in Test #4.

4. SUMMARY OF KEY OBSERVATIONS

ICET Test #4 ran for 30 days, and all conditions were maintained within the accepted flow and temperature ranges, with two exceptions. On Day 11, a power outage occurred which caused a recirculation pump trip. Recirculation flow was re-established 2 hours and 15 minutes later. During that time, the maximum solution temperature rose to 62.4ºC, which is 0.4ºC above the target maximum. The maximum temperature was above 62.0ºC for approximately one hour. The test solution pH varied from 9.5 to 9.8 over the first two days, rose to 9.9 on Day 8, and then stayed between 9.7 and 9.9 for the remainder of the test. The test solution turbidity decreased to less than 3 NTU after 24 hours. The turbidity continued to decrease and averaged 0.5 NTU over the last three weeks of the test.

Samples of the solution were taken daily. The chemical elements present were calcium, silica, and sodium. Aluminum was present for only the first 24 hours and then only at trace amounts. Strain-rate viscosity measurements indicated that the solution remained Newtonian throughout the test. No precipitates were observed in the solution, even after it had cooled to room temperature.

The submerged metal coupons were relatively unchanged, with light deposits and color changes observed. The IOZ-coated steel coupons had an average weight gain of 2.3 g, and the other metal coupons weight gains were less than 1 g. According to SEM/EDS results, the dominant corrosion products on the submerged Al coupons are likely aluminum hydroxide with other substances containing Si, Ca, O, and C. The other submerged coupons were covered with oxides, hydroxides, and other unidentified compounds. The unsubmerged coupons exhibited some vertical streaking and color changes. The IOZ-coated steel coupons had an average weight gain of 1.1 g, and the other metal coupons weight gains were less than 1 g.

Deposits on the fiberglass samples increased over time, and the deposits appeared to be chemically originated for the samples not lying on the tank bottom. These deposits covered individual fiberglass strands and in some cases formed webs between strands. The deposits did not significantly increase with time in the test solution. It is likely that these deposits were caused by chemical precipitation, since they appear to be soluble. Particulate deposits were evident on samples that were sitting on the tank bottom

In general, particulate deposits were found only on the exterior of the fiberglass. This result suggests that almost all of the particulate deposits were physically retained or attached on the fiberglass exterior. The amount of particulate deposits increases from Day-15 low- and high-flow to the Day-30 high-flow samples. EDS results show that these particulate deposits contain significant amounts of Si and Ca, suggesting they were from cal-sil debris.

Sediment on the tank bottom was prevalent, accumulating to depths of over 8 in. The sediment contained crystalline substances and calcite, making it primarily cal-sil, although some fugitive fiberglass was also present.

REFERENCES

1. “Test Plan: Characterization of Chemical and Corrosion Effects Potentially Occurring Inside a PWR Containment Following a LOCA, Rev. 12c,” March 30, 2005.

2. J. Dallman, J. Garcia, B. Letellier, and K. Howe, “Integrated Chemical Effects Tests: Data Compilation for Test 1,” LA-UR-05-0124, July 2005.

3. “Pre-Test Operations, Test #4,” ICET-PI-015, Rev. 0, May 23, 2005.

4. “Test Operations, Test #4 (cal-sil and fiberglass, and NaOH at pH 10),” ICET-PI-016, Rev. 0, May 23, 2005.

5. “Post-Test Operations, Test #3,” ICET-PI-008, Rev. 3, May 2, 2005.